

Cite this: *J. Mater. Chem. A*, 2018, **6**, 574

Modulation of the power conversion efficiency of organic solar cells *via* architectural variation of a promising non-fullerene acceptor†

Ruchika Mishra,^a Ramprasad Regar,^a Varun Singh,^a Piyush Panini,^a Rahul Singhal,^b M. L. Keshtov,^c Ganesh D. Sharma^{b,d} and Jeyaraman Sankar^{b,*a}

Thiophene-containing molecular materials are recognised as efficient substrates in organic photovoltaics. Herein, we have demonstrated the effect of substitution patterns of thiophenes on the electron accepting ability of perylene bisimide derivatives, which in turn dictates the photovoltaic performance. The thiophene units were integrated through α - or β -positions on the 1- or 1,7-bay positions of perylene-bisimide through alkyne spacers in order to modulate the electronic properties of PBI. The target molecules are structurally robust as per electrochemical studies and exhibited broad absorption in the visible region. Better light harvesting ability and favourable LUMO energy levels render these dyads and triads suitable as electron acceptors in organic solar cells. Bulk heterojunction solar cells were constructed from thienyl-PBI (1–4) as acceptors and a polymer P as a donor. α -Linked 1 and 3 showed a PCE of 5.72% and 6.94% with a remarkable energy loss of 0.55 eV and 0.58 eV, respectively whereas, β -linked 2 and 4 showed an overall PCE of 4.93% and 6.06% with an energy loss of 0.52 eV and 0.54 eV, respectively.

Received 27th September 2017
Accepted 4th December 2017

DOI: 10.1039/c7ta08533h

rsc.li/materials-a

Introduction

Organic photovoltaics (OPVs) have emerged as a promising cost-effective alternative for harnessing solar energy efficiently owing to their tunable absorption, mechanical flexibility, light weight and easier functionalization.^{1–4} Organic solar cells (OSCs) based on solution-processed bulk heterojunctions (BHJs) with small molecules as a donor-acceptor blend in the absorber active layer are instrumental in attaining high power conversion efficiency (PCE).^{4–7} Most of the highly efficient BHJ OSCs reported so far employ fullerene derivatives (PC₆₁BM and PC₇₁BM) as acceptors. High electron affinity and isotropic charge transport with remarkable electron mobility render fullerene an ideal acceptor for the best performing devices.^{8–15} Nevertheless, fullerene-based acceptors have certain inherent downsides such as poor light harvesting in the visible region,

high cost, less tunable architecture, morphological instability in thin films and large energy loss, thus limiting further improvement in the PCE.¹⁶ Thus, in order to circumvent these issues, the development of new non-fullerene small molecule acceptors (NFSMAs) which show PCEs comparable to or even higher than that of fullerene, has gained large momentum over the past decade.^{17–21} Compared with fullerene-based acceptors, NFSMAs possess efficient absorption and tunable molecular structures. In most cases, NFSMAs are derivatives of electron acceptors with a larger π -surface having the advantage of better charge delocalization and transport. Generally, these electron acceptors have a low lying LUMO with n-type semiconductivity.^{22–24} Recently, the overall PCE of PSCs based on NFSMAs has reached the range of 12–13%.^{25,26}

Among the non-fullerene acceptors, perylene bisimide (PBI) derivatives^{27–30} have drawn much attention owing to their n-type semiconductivity, higher thermochemical stability, larger π -conjugated backbone and superior photophysical properties. Unlike fullerenes, PBI derivatives exhibit strong absorption in the visible region between 400 nm and 650 nm, high electron mobilities, low lying LUMO energy levels, and flexibility in design and hence, they are widely explored as small molecule acceptors for BHJ OSCs.³¹ However, because of the large planar structure of the perylene core, the unfunctionalized PBI molecules often show a high aggregation tendency in thin films, leading to large crystallization domains over 20 nm (ref. 32) and may limit exciton dissociation,³³ thereby hampering the device performance. The solution processability of PBIs can be improved by introducing bulky groups onto the *N*-, *bay*- and/or *ortho*-positions of PBI.^{34–44}

^aDepartment of Chemistry, Indian Institute of Science Education and Research (IISER) Bhopal, Bhopal Bypass Road, Bhauri, Bhopal, Madhya Pradesh, India – 462066. E-mail: sankar@iiserb.ac.in

^bDepartment of Physics, Malviya National Institute of Technology, Jaipur, Rajasthan, India – 302031

^cInstitute of Organoelement Compounds of the Russian Academy of Sciences, Vavilova St., 28, 119991 Moscow, Russian Federation

^dDepartment of Physics, The LNM Institute of Information Technology, A Deemed University, Jamdoli, Jaipur, Rajasthan, India - 302031. E-mail: gdsharma273@gmail.com

† Electronic supplementary information (ESI) available. CCDC 1042505 and 1569915. For ESI and crystallographic data in CIF or other electronic format see DOI: 10.1039/c7ta08533h

This further helped in achieving remarkable PCEs for OSCs using the PBI-based acceptors (Chart 1).^{15,45–49} Thiophene units on the other hand are highly sought after substituents for developing organic functional materials.^{50–53}

These are good substituents to improve the solubility and have excellent donor properties with inherent electron delocalization. If PBI and thiophene can be incorporated into a single molecular framework, the electronic properties can be manipulated to achieve promising materials for OSCs.

In this context, we designed and synthesized a series of PBI based small molecule acceptors (**1–4**) for bulk heterojunction solar cells. The molecules **1** and **3** have a thiophene moiety connected through the α -position to the 1- and 1,7-positions of the PBI bay area respectively whereas in the case of **2** and **4**, it is attached *via* a β -linkage to the 1- and 1,7-positions of the PBI bay area respectively (Chart 2). The π -linker has pronounced effects on the molecular conformation and electronic distribution of the D–A type molecular system.³⁴ Therefore, an alkyne linker was chosen to make sure that the thiophene and PBI units remain co-planar for better orbital overlap, which would result in improved electronic communication.

These small molecules were used as electron acceptors along with a low bandgap D–A copolymer⁵⁴ **P** (Chart 2) as an electron donor with broad absorption. **P** has an optical bandgap of 1.56 eV with HOMO and LUMO energy levels around -5.25 eV and -3.72 eV, respectively. The photovoltaic performances of these OSCs assembled from the abovementioned D–A pairs were found to be highly dependent on the linkage position and conjugation length, subsequently influencing the resulting PCEs. Recrystallization from hexane/ CHCl_3 afforded analytically pure compounds **1–4**. All the synthesized molecules were characterized by NMR spectroscopy as well as by atmospheric pressure chemical ionization high resolution mass spectrometry (APCI-HRMS). Complete synthetic and characterization details of the precursors and newly synthesized molecules are provided in the ESI.†

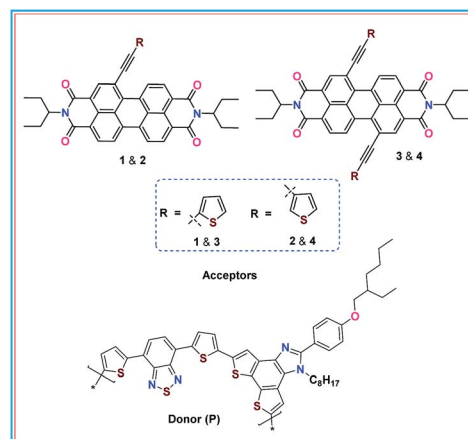


Chart 2 Schematic representation of **1–4**.

Device fabrication and characterisation

The device structure was ITO/PEDOT:PSS/active layer/PFN/Al. The indium tin oxide (ITO) coated glass substrates were cleaned with an ultrasonication process sequentially in detergent, deionized water, acetone and isopropyl alcohol and then dried under ambient conditions. After filtration through a 0.45 μm filter, PEDOT:PSS (Bay P VP AI 4083, Bayer AG) was spin-coated at 3500 rpm for 60 s to form a 40 nm thick layer on the cleaned ITO substrate, and baked on a hot plate at 120 $^\circ\text{C}$ for about 10 min. A blend mixture of **P–1** or **2** or **3** or **4** (different weight ratios of 1 : 0.5, 1 : 1, 1 : 1.5, 1 : 2 and 1 : 2.5) was prepared using chloroform (total concentration of 18 mg mL^{-1}) and then its thin film of about 90 ± 5 nm was deposited on the top of the PEDOT:PSS layer by spin coating at 1500 rpm for 60 s. For solvent vapor annealing (SVA), the above-prepared active layers were placed in a Petri dish containing chloroform for 60 s. After that 0.5 mg mL^{-1} of PFN in MeOH was directly spin-coated on the active layer at 4000 rpm for 40 s. An aluminium (Al) cathode (70 nm) was then evaporated onto the surface of the photoactive layer with or without a surface interface layer under high vacuum (10^{-5} mbar) to form the cathode. Hole-only and electron-only devices were fabricated similarly to the PSCs with a structure of ITO/PEDOT:PSS/active layer/Au and ITO/Al active layer/Al, respectively. The J – V characterization of the devices was carried out on a computer-controlled Keithley 2400 Source Measurement system. A solar simulator was used as the light source, and the light intensity was monitored by using a standard Si solar cell. The incident photon-to-current efficiency (IPCE) of the devices was measured by illuminating the devices with the light source and a monochromator and the resulting current was measured using a Keithley electrometer under short-circuit conditions.

Results and discussion

Synthesis

The synthetic pathways are displayed in Scheme 1. To install an ethyne group, we chose to employ a typical Sonogashira

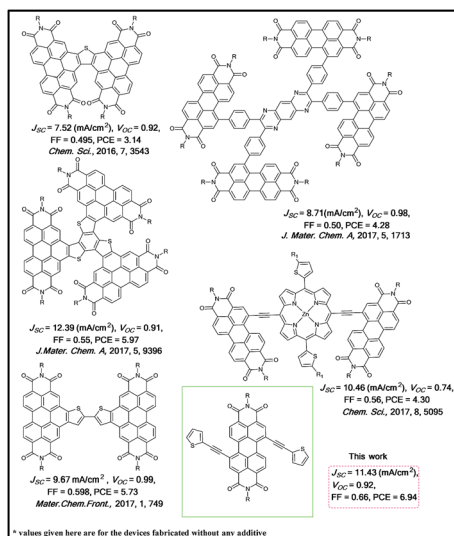
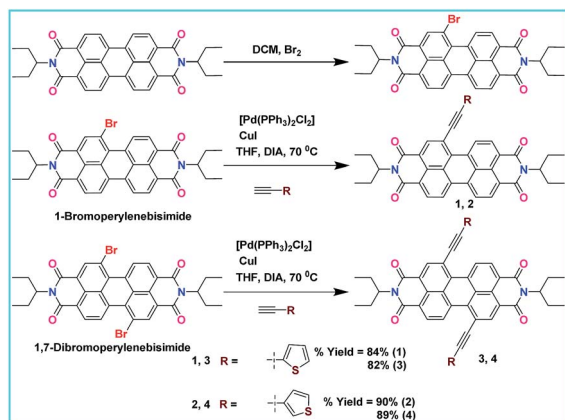


Chart 1 Selective acceptors based on perylene bisimides reported recently.



Scheme 1 Synthesis of dyads 1–4 via Sonogashira coupling.

coupling reaction between ethynylthiophene and 1-bromo or 1,7-dibromoperylene bisimide.^{55,56}

Absorption and emission studies

The steady-state absorption of the PBI derivatives 1–4 was recorded from 10^{-6} M solution in CHCl_3 . The absorption profiles of compounds 1–4 reveal a prominent red shift compared to unsubstituted PBI in their π - π^* transition along with band broadening (Fig. 1).

In the case of mono-substituted dyads 1 ($\lambda_{\text{max}}^{\text{abs}} = 556$ nm) and 2 ($\lambda_{\text{max}}^{\text{abs}} = 549$ nm), absorption maxima showed bathochromic shifts of ~ 30 nm and 20 nm respectively compared to that of parent PBI. 1,7-Bis(ethynyl-thienyl) PBI derivatives 3 ($\lambda_{\text{max}}^{\text{abs}} = 587$ nm) and 4 ($\lambda_{\text{max}}^{\text{abs}} = 575$ nm) displayed the most interesting absorption features with remarkable red shifts of around 70 nm and 60 nm respectively (Table 1).

The above observations are attributed to the overall planarity achieved in these systems, which further extends the conjugation and narrows the band gap. Interestingly, compounds 1 and 3, in which thiophene is attached through the α -position, exhibit larger bathochromic shifts than β -linked 2 and 4. Experimental band gaps obtained from the optical data confirm the conjugation extension. The absorption spectra of thin films of 1–4 are shown in Fig. 1. It can be seen from Fig. 1 that the absorption band is slightly red shifted and broadened in comparison to that in solution, suggesting stacking interactions in the solid state. The optical bandgaps estimated from the absorption edge in thin films are found to be 1.92 eV, 1.98 eV, 1.86 eV and 1.94 eV, for 1, 2, 3 and 4 respectively. The optical absorption spectra of conjugated polymer P in the thin film showed an absorption band centred at 670 nm (Fig. S16, ESI[†]) which is complementary to the absorption spectra of PBIs, indicating that both P and PBIs contribute to the photocurrent generation in resultant OSCs. To gain further insights into the role of the thienyl substituents on the optical properties of PBI, emission studies were conducted on chloroform solutions of 1–4 (Fig. 2). Altering the thiophene position over the linker significantly modifies the characteristic emission profile of PBI. The emission profiles of all the molecules are red

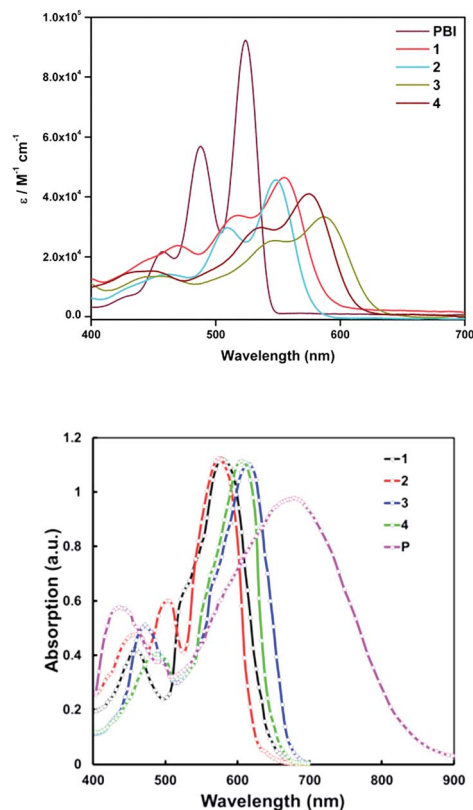


Fig. 1 Absorption spectra of molecules 1–4 in chloroform (top) and in thin films (bottom).

shifted with complete loss of vibronic progression relative to the vibronically discernible emission features of parent PBI.

Emission maxima for these molecular systems are red shifted in the region 550–670 nm (Table 1). Mono-thienyl appended PBIs appeared to be more fluorescent than dithienyl analogues. Fluorescence quantum yields (Φ) were estimated to be ~ 0.4 for 1 and 2 which were reduced to ~ 0.2 and ~ 0.3 respectively for 3 and 4. Steady state absorption and emission features further corroborate the influence of the thienyl architecture on the optical properties. Solvent dependent absorption spectra show a blue shift in absorption maxima with fluorescence quenching in polar solvents (Fig. S17[†]).

Table 1 Optical and electrochemical data

Compound	$\lambda_{\text{max}}^{\text{abs}}$ (nm)	$\epsilon/10^5$ ($\text{M}^{-1} \text{cm}^{-1}$)	$\lambda_{\text{max}}^{\text{em}}$ (nm)	E_{red} (V)
1	556	0.47	594	−0.66 −0.79
2	549	0.46	578	−0.66 −0.79
3	587	0.33	622	−0.59 −0.71
4	575	0.42	603	−0.62 −0.73

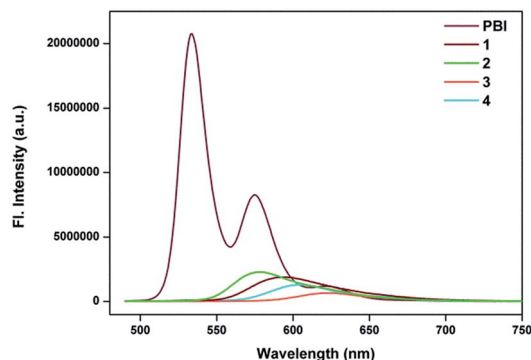


Fig. 2 Emission spectra of molecules 1–4 in chloroform.

Single crystal X-ray diffraction studies

To comprehend the photophysical data obtained for the present set of molecules, a thorough structural investigation was imminent and therefore efforts were taken to structurally characterize 1–4. Initial efforts to obtain X-ray quality single crystals were not successful. Single crystals suitable for X-ray diffraction studies could be grown only for 1 and 4 after repetitive trials.

From Fig. 3, it can be seen that the thienyl moiety is perfectly coplanar with the PBI aromatic core without any core distortion. Thus, the planarity of the entire π -system is conserved which is necessary in order to ascertain the observed microscopic and photophysical properties. A careful analysis of the X-ray diffraction data provided further information on the stacking interactions in the solid state. Every molecule of 4 is stacked between four molecules in a sandwich fashion. This arrangement provides ample scope for the aryl moieties to have a number of π - π stacking interactions. Fig. 3 depicts one such stacking in which a thiophene unit is stacked over the core of the PBI resulting in π - π interactions having a distance of 3.56

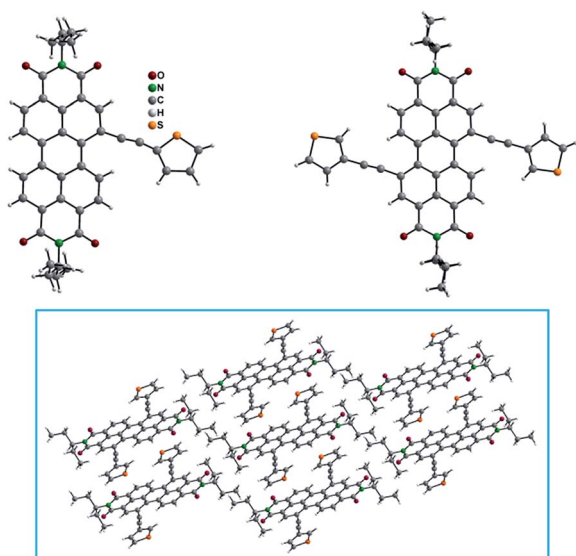


Fig. 3 Single-crystal X-ray diffraction structure of 1 (CCDC 1569915) & 4 (CCDC 1042505) & packing diagram of 4 (below).

Å. The presence of extensive stacking hints at the possibility of efficient charge carrier mobilities. Further details about the packing and torsion angles are provided in the ESI.†

Computational investigations

DFT calculations performed at the B3LYP/6-311g** level using Gaussian 09 suite of programs⁵⁷ suggest that the HOMO is delocalized over the whole PBI and thienyl framework in all four molecules. The LUMO, on the other hand, is localized only over the PBI framework with limited delocalization on the alkyne-bridge (Fig. 4). These data corroborated the fact that the conjugation extension has been made feasible by the alkynyl linker.^{34,55} In addition to the extended conjugation, the presence of sulphur contributes towards the red shift.

Electrochemical investigations

All molecules 1–4 showed two characteristic reversible reductions in the range of 0.6–0.8 V vs. the SCE (Table 1) in cyclic voltammetric studies.

An easier reduction in all these cases points to the possibility of π -extension with respect to PBI. The second reduction was more facile in the case of 1,7-di substituted thienyl PBIs 3 and 4 than that in 1-thienyl PBIs 1 and 2 (Fig. 5). Similarly, in 3 and 4, the ease of reduction compared to 1 and 2 hints at more delocalisation of the π -cloud upon bay di-substitution.³⁴

The HOMO and LUMO energy levels of these small molecules were estimated from CV data (Fig. 5). HOMO energy levels for the β -linked derivatives are slightly up-shifted compared to α -linked counterparts, whereas the LUMO energy levels of β -linked derivatives get deepened. The LUMO energy levels of the derivatives 1–4 are higher than that of PC₇₁BM, which is beneficial in attaining the high V_{oc} of the resulting OSCs. To add further, the HOMO offset between these acceptors and the P donor is higher than the threshold value of 0.3 eV which ensures that the hole transfer from 1–4 to P donor is feasible in the active layer. On the other hand, the LUMO offset is below the threshold value (0.3 eV), warranting efficient electron transfer from P to PBI acceptors (1–4).

Photoluminescence quenching

Photoluminescence (PL) spectra of pristine P and 1–4 in thin films were recorded to investigate the charge transfer in OSCs.

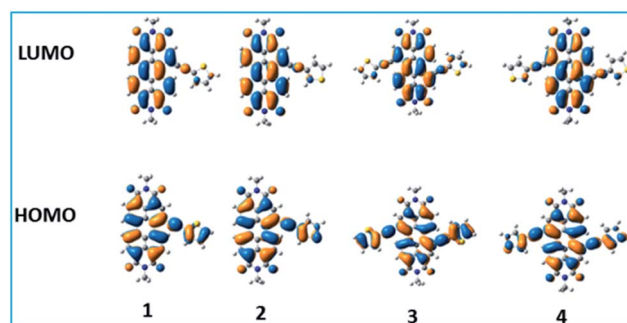


Fig. 4 Frontier orbital pictures of compounds 1–4.

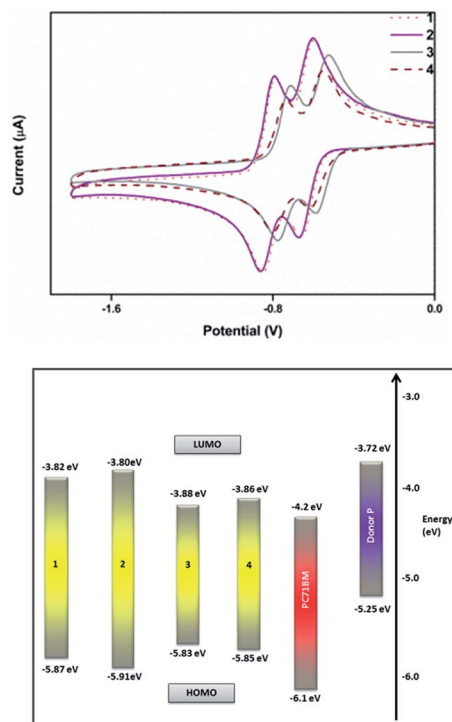


Fig. 5 Cyclic voltammograms of the molecules 1–4 in DCM (Top) & Frontier energy levels of 1–4 in comparison to PC₇₁BM (Bottom).

PL quenching experiments were carried out at an excitation wavelength of 660 nm. The PL emission of **P** was located at 812 nm while PBI derivatives 1–4 displayed emission in the range of 590–630 nm. **P**:PBI derivative (1–4) (weight ratio 1 : 2) blended films (Fig. 6) showed quenching of PL. As shown in Fig. 6 the quenching efficiencies of the polymer donor and α -linked PBI acceptors (**P**:1 and **P**:3) decreased by 92% and for β -linked PBI (**P**:2 and **P**:4) the quenching efficiency decreased by 88%. The stronger PL quenching suggests more efficient photo-induced charge transfer in **P**:1 or 3 blends than that in **P**:2 or 4 blends.

Photovoltaic properties

To probe the photovoltaic performances of these derivatives, BHJ-OSCs were fabricated using a conventional device structure of ITO/PEDOT:PSS/**P**:PBI (1–4)/PFN/Al (the details of device fabrication and characterization are described in the ESI†). The optimized active layers were obtained by spin-casting from a chloroform solution. Organic solar cells prepared from a 1 : 2 weight ratio of donor (**P**) and acceptor (1–4) showed the best photovoltaic performance.

The OSCs based on mono-substituted 1 and 2 revealed an overall PCE of 3.25% and 2.81%, respectively with a V_{oc} of 1.04 V, whereas, di-substituted 3 and 4 showed an overall PCE of 3.36% and 3.14%, with a V_{oc} of 0.98 V (Table S1, ESI†). The higher values of V_{oc} for the OSCs based on 1 and 2 relative to 3 and 4 can be ascribed to the high lying LUMO energy levels of 1 and 2 as compared to 3 and 4, since the V_{oc} of BHJ-OSCs is directly proportional to the energy difference between the

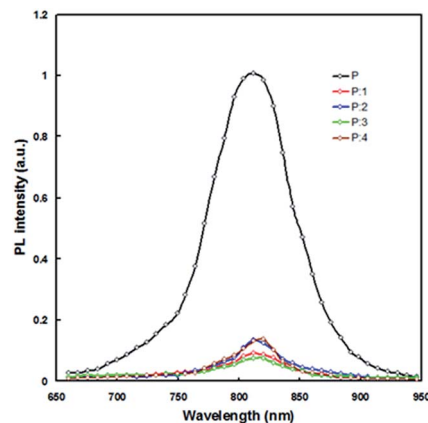


Fig. 6 PL spectra of thin film blends from donor **P** and acceptors 1–4.

HOMO level of the donor and the LUMO level of the acceptor employed in the active layer.

The higher values of J_{sc} for OSCs (Table S1, ESI†) based on 3 and 4 compared to 1 and 2 counterparts may be related to a slightly larger LUMO offset between the formers and **P** indicating more efficient exciton dissociation in the devices based on di-substituted 3 and 4. The PL spectra show that PL quenching is more for **P**:1 and **P**:3 blend films than that for **P**:2 and **P**:4 and also confirm the more efficient charge transfer in OSCs based on the former blends than the latter.

Although the LUMO offset for PBI (1–4):**P** is about 0.10–0.16 eV, which is lower than the threshold value 0.3 eV, the electron transfer from donor **P** to PBI acceptors seems to be efficient, as confirmed from the PL quenching measurements. Recent studies have proven that efficient charge separation can occur despite an energy offset smaller than 0.3 eV.^{58,59}

In order to improve the PCE of the above devices, we have employed SVA treatment of active layers. The current–voltage characteristics of the devices based on optimised active layers are shown in Fig. 7 and the photovoltaic parameters are compiled in Table 2. SVA treatment played a positive role in enhancing the PCEs of the OSCs. The devices based on mono-substituted 1 and 2 showed an overall PCE of 5.72% and 4.93%, respectively, whereas their di-substituted counterparts 3

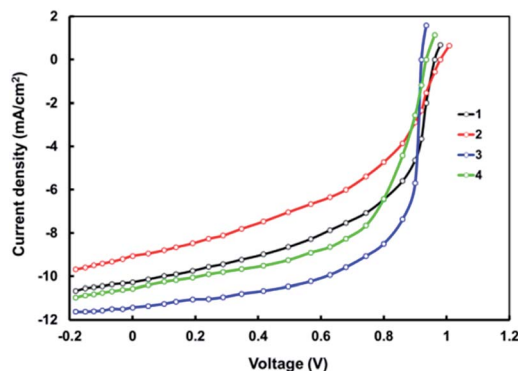


Fig. 7 Current density vs. voltage (J – V) characteristics of the devices based on 1–4 under AM1.5 G irradiation (100 mW cm^{-2}).

Table 2 Photovoltaic parameters of organic cells fabricated using 1–4 via SVA treatment under the illumination of AM 1.5G, 100 mW cm⁻²

Compound	J_{sc} (mA cm ⁻²)	V_{oc}	FF	PCE (%)	μ_h (cm ² V ⁻¹ s ⁻¹) × 10 ⁻⁴	μ_e (cm ² V ⁻¹ s ⁻¹) × 10 ⁻⁴
1	10.27 (10.16) ^b	0.96	0.58	5.72 (5.61) ^a	1.16 (±0.05)	4.15 (±0.07)
2	9.06 (8.97) ^b	0.99	0.55	4.93 (4.84) ^a	1.11 (±0.07)	3.12 (±0.05)
3	11.43 (11.36) ^b	0.92	0.66	6.94 (6.89) ^a	1.18 (±0.04)	4.64 (±0.04)
4	10.57 (10.43) ^b	0.94	0.61	6.06 (5.92) ^a	1.13 (±0.05)	4.21 (±0.05)
PC ₇₁ BM	6.34	0.84	0.42	2.24		

^a Average performance values out of 8 devices. ^b Estimated from the IPCE spectra.

and 4 showed an overall PCE of 6.94% and 6.06%. We have also used 3 as an acceptor and a well-known polymer P3HT as a donor and achieved an overall PCE of 6.07% with $J_{sc} = 10.63$ mA cm⁻², $V_{oc} = 0.84$ V and FF = 0.68. The increase in PCE for the OSCs is attributed to the substantial increase in both J_{sc} and FF with a slight reduction in V_{oc} . We further measured the incident photon-to-current conversion efficiency (IPCE) of these devices and IPCE spectra are shown in Fig. 8. From Fig. 8, it is clear that the spectra are broader over the entire visible region from 350–850 nm.

The close resemblance of the IPCE spectra to the absorption spectra of corresponding P:PBIs (1–4) active layers (Fig. S18, ESI†) is indicative of a complementary contribution of both the conjugated polymer donor and PBIs to the J_{sc} values. Fig. 8 shows that IPCE values for the devices based on 1 and 3 active layers were higher than those of 2 and 4. This is indicative of a highly efficient photoelectron conversion process in the former devices than that in the latter ones and also confirms the higher value of J_{sc} for the devices based on 1 & 3 than 2 & 4 counterparts.

High IPCE values in the 650–800 nm region (where the light absorption is mainly ascribed to the donor P) illustrate effective electron transfer from donor P to acceptors 1–4 despite the low LUMO energy offset. The J_{sc} values estimated from IPCE spectra are 10.16 mA cm⁻², 8.97 mA cm⁻², 11.36 mA cm⁻², and 10.43 mA cm⁻² respectively for 1–4 based devices. These values are within a reasonable mismatch to the J_{sc} values estimated from the corresponding J - V curves under illumination.

The V_{oc} of an organic solar cell is dependent on the LUMO energy level of the acceptor. The devices based on non-fullerene acceptors 1–4 (P:PBI (1–4)) displayed V_{oc} in the range of 0.93 to 0.99 V which is much higher than that of the device constructed from donor P and a fullerene-based acceptor PC₇₁BM (P:PC₇₁BM), due to the up-shift in the LUMO energy level of PBIs, relative to PC₇₁BM.

The hole mobility (μ_h) and electron mobility (μ_e) of the blended active layers based on 1, 2, 3 and 4 were measured from the dark J - V characteristics of electron-only and hole-only devices using the space charge limited current model. Since the hole mobilities for all the active layers remained similar (about an average value of 1.14×10^{-4} cm² V⁻¹ s⁻¹), we have only observed dark J - V characteristics for electron-only devices (Fig. 9 and Table 2). The electron mobilities follow the trend 3 > 4 > 1 > 2, indicating that the electron mobility for the α -linked PBI is higher than that for β -linked PBI. Moreover the D- π -A- π -D PBI showed higher electron mobility than the D- π -A counterpart. These results demonstrated more balanced charge transport in the devices made from α -linked PBIs than from β -linked PBIs. In order to investigate the charge generation and transport properties of the OSCs, the variation of photocurrent (J_{ph}) with effective voltage (V_{eff}) was measured (Fig. 10). $J_{ph} = J_L - J_D$, where J_L and J_D are the current densities under illumination and under dark, respectively, and $V_{eff} = V_o - V_a$, where V_o is the voltage when J_{ph} is zero, and V_a is the applied voltage. From Fig. 10 it can be envisaged that when V_{eff} is sufficiently high, J_{ph}

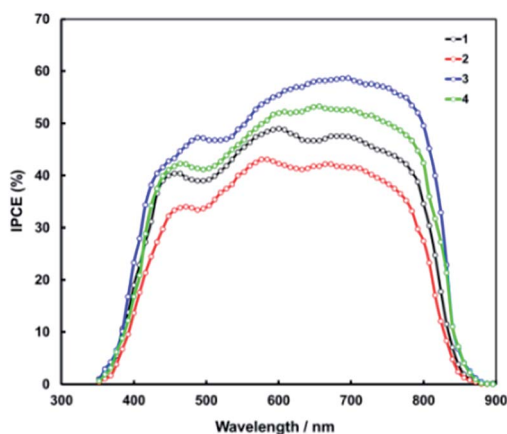
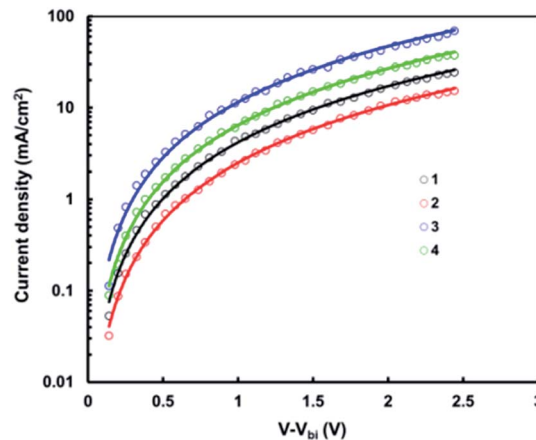


Fig. 8 IPCE spectra of solar cells corresponding to 1–4.

Fig. 9 J - V curves of the electron-only devices for the optimized active layers of 1–4.

becomes saturated (J_{sat}) and all the photogenerated excitons are dissociated into free charge carriers and collected by the electrodes. J_{sat} is only limited by the total amount of incident photons and the ratio $J_{\text{ph}}/J_{\text{sat}}$ provides information about the exciton dissociation efficiency and charge collection efficiency.^{60–63}

As can be seen from Fig. 10, although the J_{sat} values for all OSCs remain mostly the same, the J_{ph} values for the devices based on **3** are the largest at certain V_{eff} before J_{ph} is saturated and the trend is $3 > 4 > 1 > 2$. We have estimated the exciton dissociation and charge collection efficiency under short circuit conditions and are about 0.87, 0.85, 0.92 and 0.89 for **1**, **2**, **3** and **4** based devices, respectively. This suggests that OSCs based on acceptor **3** show the highest dissociation efficiency or charge collection efficiency among all devices. The higher charge collection efficiency also indicates a lower bimolecular recombination that is responsible for a larger FF value. Besides, the device based on **2** shows a strong field dependence across the largest V_{eff} range and J_{ph} becomes slightly saturated at V_{eff} values more than 1.4 V, but the J_{ph} value of the **3** based device is almost saturated at a much lower V_{eff} value around 0.5 V, which suggests that photogenerated excitons can be more efficiently dissociated into free charge carriers and subsequently collected at the electrode with suppressed bimolecular recombination, leading to larger FF values in **3** based devices.⁶⁴

Low energy loss (E_{loss}) is another notable characteristic associated with the SCs based on acceptors **1–4**. The E_{loss} is defined as $E_{\text{loss}} = E_g - qV_{\text{oc}}$, where E_g is the optical band gap of either the donor or acceptor employed in the active layer of PSCs, whichever is smaller.⁶⁵ Here E_g is the optical bandgap of the donor polymer. Lower energy loss subsequently leads to a high J_{sc} and PCE. The energy loss (E_{loss}) observed for **1–4** remained in the range of 0.52 to 0.58 eV, which is lower than that observed for OSCs based on the fullerene acceptor and is in line with that of the non-fullerene acceptor based devices with low driving force less than 0.3 eV.^{66–70} The E_{loss} in our devices based on PBI acceptors, is one of the lowest values for BHJ-OSCs. The low energy loss may be related to the higher values

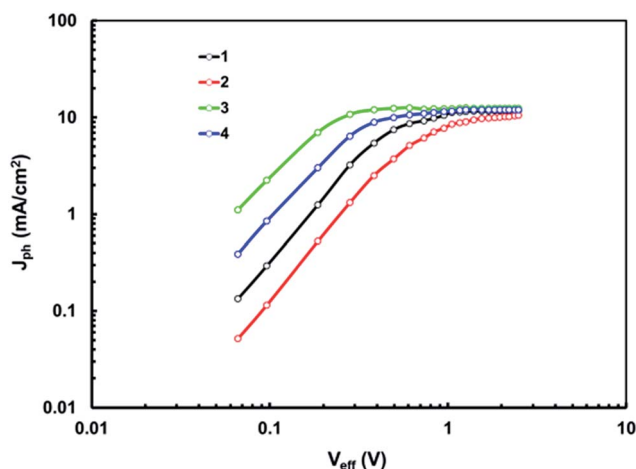


Fig. 10 Variation of photocurrent density (J_{ph}) with effective voltage (V_{eff}) for the optimized devices based on **1–4**.

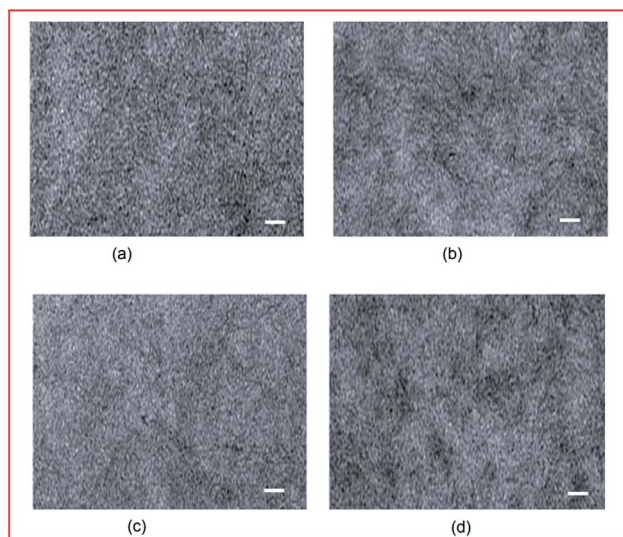


Fig. 11 TEM images of optimized (a) P:1, (b) P:2, (c) P:3 and (d) P:4 thin films, scale bar 200 nm.

of LUMO energy levels and the low LUMO offset and HOMO offset between the donor and the acceptor and is beneficial for obtaining high V_{oc} .

The morphologies of the optimized active layers were investigated using transmission electron microscopy (TEM) (Fig. 11). It can be seen from Fig. 11 that all the optimized blend thin films showed uniform morphology with no large domains. Among all the blend films, **P:1** and **P:3** films exhibited increased nano-fibrils and more desired bi-continuous interpenetrating networks between donor **P** and acceptors **1–4**, benefiting charge generation and transportation, and thereby leading to enhanced J_{sc} and FF with suppressed charge recombination.^{71,72}

Conclusions

In summary, four thienyl-perylene bisimide derivatives (**1–4**), in which thienyl units were substituted at α or β positions on the 1- and 1,7-positions of perylene-bisimide through alkyne spacers, were synthesized and their optical and electrochemical properties were investigated. These materials have been exploited as non-fullerene acceptors for the fabrication of solution processed organic solar cells. The photovoltaic devices based on **P:1**, **P:2**, **P:3** and **P:4** exhibit an overall PCE of 5.72%, 4.93%, 6.94% and 6.06% respectively, with V_{oc} values between 0.92 and 0.99 V. An impressive energy loss in the range of 0.52–0.58 eV was also observed which is in the rank of the best known values. These results confirmed that the linkage position along with extended conjugation has a significant impact on the photovoltaic performance of the devices. Our results also demonstrate that the PCE of the OSCs based on these PBI acceptors can be easily tailored by judicious choice of substituents.

Conflicts of interest

There are no conflicts to declare.

Acknowledgements

We thank CREST-MHRD, IISER Bhopal and DST-SERB EMR/2016/005768 for funding. RR thanks DST for the INSPIRE fellowship.

References

- 1 C. Brabec, U. Scherf and V. Dyakonov, *Organic Photovoltaics: Materials, Device Physics, and Manufacturing Technologies*, Wiley-VCH Verlag GmbH & Co. KGaA, Weinheim, Germany, 2nd edn, 2014.
- 2 A. J. Heeger, *Adv. Mater.*, 2013, **26**, 10–28.
- 3 F. C. Krebs, N. Espinosa, M. Hösel, R. R. Søndergaard and M. Jørgensen, *Adv. Mater.*, 2013, **26**, 29–39.
- 4 L. Ye, S. Zhang, L. Huo, M. Zhang and J. Hou, *Acc. Chem. Res.*, 2014, **47**, 1595–1603.
- 5 G. Yu, J. Gao, J. C. Hummelen, F. Wudl and A. J. Heeger, *Science*, 1995, **270**, 1789.
- 6 A. Mishra and P. Bauerle, *Angew. Chem., Int. Ed.*, 2012, **51**, 2020–2067.
- 7 J. Kesters, P. Verstappen, M. Kelchtermans, L. Lutsen, D. Vanderzande and W. Maes, *Adv. Energy Mater.*, 2015, **5**, 1500218.
- 8 V. Vohra, K. Kawashima, T. Kakara, T. Koganezawa, I. Osaka, K. Takimiya and H. Murata, *Nat. Photonics*, 2015, **9**, 403–408.
- 9 B. Kan, Q. Zhang, M. Li, X. Wan, W. Ni, G. Long, Y. Wang, X. Yang, H. Feng and Y. Chen, *J. Am. Chem. Soc.*, 2014, **136**, 15529–15532.
- 10 S. D. Collins, N. A. Ran, M. C. Heiber and T. Q. Nguyen, *Adv. Energy Mater.*, 2017, 1602242.
- 11 P. Fu, X. Guo, B. Zhang, T. Chen, W. Qin, Y. Ye, J. Hou, J. Zhang and C. Li, *J. Mater. Chem. A*, 2016, **4**, 16824–16829.
- 12 Y. Jin, Z. Chen, S. Dong, N. Zheng, L. Ying, X. F. Jiang, F. Liu, F. Huang and Y. Cao, *Adv. Mater.*, 2016, **28**, 9811–9818.
- 13 X. Liu, X. Li, Y. Li, C. Song, L. Zhu, W. Zhang, H. Q. Wang and J. Fang, *Adv. Mater.*, 2016, **28**, 7405–7412.
- 14 L. Nian, K. Gao, F. Liu, Y. Kan, X. Jiang, L. Liu, Z. Xie, X. Peng, T. P. Russell and Y. Ma, *Adv. Mater.*, 2016, **28**, 8184–8190.
- 15 Q. Wan, X. Guo, Z. Wang, W. Li, B. Guo, W. Ma, M. Zhang and Y. Li, *Adv. Funct. Mater.*, 2016, **26**, 6635–6640.
- 16 M. C. Scharber, *Adv. Mater.*, 2016, **28**, 1994–2001.
- 17 Y. Lin and X. Zhan, *Mater. Horiz.*, 2014, **1**, 470–488.
- 18 W. Chen and Q. Zhang, *J. Mater. Chem. C*, 2017, **5**, 1275–1302.
- 19 H. Y. Li, T. Earmme, G. Q. Ren, A. Saeki, S. Yoshikawa, N. M. Murari, S. Subramanian, M. J. Crane, S. Seki and S. A. Jenekhe, *J. Am. Chem. Soc.*, 2014, **136**, 14589–14597.
- 20 C. B. Nielsen, S. Holliday, H.-Y. Chen, S. J. Cryer and I. McCulloch, *Acc. Chem. Res.*, 2015, **48**, 2803–2812.
- 21 S. S. Li, Y. Li, W. C. Zhao, S. Q. Zhang, S. Mukherjee, H. Ade and J. H. Hou, *Adv. Mater.*, 2016, **28**, 9423–9429.
- 22 Y. Lin and X. Zhan, *Adv. Energy Mater.*, 2015, **5**, 1501063; Y. Lin and X. Zhan, *Acc. Chem. Res.*, 2016, **49**, 175–183.
- 23 Y. Lin, J. Wang, Z.-G. Zhang, H. Bai, Y. Li and D. Zhu, *Adv. Mater.*, 2015, **27**, 1170–1174.
- 24 Y. Lin, F. Zhao, Q. He, L. Huo, Y. Wu and T. C. Parker, *J. Am. Chem. Soc.*, 2016, **138**, 4955–4961.
- 25 S. J. Xu, Z. Zhou, W. Liu, Z. Zhang, F. Liu, H. Yan and X. Zhu, *Adv. Mater.*, 2017, **29**, 1704510.
- 26 W. Zhao, S. Li, H. Yao, S. Zhang, Y. Zhang, B. Yang and J. Hou, *J. Am. Chem. Soc.*, 2017, **139**, 7148–7151.
- 27 X. Zhan, Z. Tan, B. Domercq, Z. An, X. Zhang and S. Barlow, *J. Am. Chem. Soc.*, 2007, **129**, 7246–7247.
- 28 X. Zhan, A. Facchetti, S. Barlow, T. J. Marks, M. A. Ratner and M. R. Wasielewski, *Adv. Mater.*, 2011, **23**, 268–284.
- 29 H. Lin, S. Chen, H. Hu, L. Zhang, T. Ma and J. Y. Lai, *Adv. Mater.*, 2016, **28**, 8546–8551.
- 30 S. Li, W. Liu, C.-Z. Li, F. Liu, Y. Zhang and M. Shi, *J. Mater. Chem. A*, 2016, **4**(27), 10659–10665.
- 31 C. Li and H. Wonneberger, *Adv. Mater.*, 2012, **24**, 613–636.
- 32 J. J. Dittmer, E. A. Marseglia and R. H. Friend, *Adv. Mater.*, 2000, **12**, 1270–1274.
- 33 I. A. Howard, L. Frederick, P. E. Keivanidis, R. H. Friend and N. C. Greenham, *J. Phys. Chem. C*, 2009, **113**, 21225–21232.
- 34 C. Huang, S. Barlow and S. R. Marder, *J. Org. Chem.*, 2011, **76**, 2386–2407.
- 35 H. Langhals, *Heterocycles*, 1995, **40**, 477–500.
- 36 F. Würthner, *Chem. Commun.*, 2004, 1564–1579.
- 37 T. Weil, U. Wiesler, M. A. Herrmann, R. Bauer, J. Hofkens, F. C. D. Schryver and K. Mullen, *J. Am. Chem. Soc.*, 2001, **123**, 8101–8108.
- 38 A. Zhang, C. Li, F. Yang, J. Zhang, Z. Wang, Z. Wei and W. Li, *Angew. Chem., Int. Ed.*, 2017, **56**, 2694–2698.
- 39 D. Meng, D. Sun, C. Zhong, T. Liu, B. Fan, L. Huo, Y. Li, W. Jiang, H. Choi, T. Kim, J. Y. Kim, Y. Sun, Z. Wang and A. J. Heeger, *J. Am. Chem. Soc.*, 2016, **138**, 375–380.
- 40 I. Kim, H. M. Haverinen, Z. X. Wang, S. Madakuni, J. Li and G. E. Jabbour, *Appl. Phys. Lett.*, 2009, **95**, 023305.
- 41 R. Shivanna, S. Shoaee, S. Dimitrov, S. K. Kandappa, S. Rajaram, J. R. Durrant and K. S. Narayan, *Energy Environ. Sci.*, 2014, **7**, 435–441.
- 42 X. Zhang, B. Jiang, X. Zhang, A. Tang, J. Huang and C. Zhan, *J. Phys. Chem. C*, 2014, **118**, 24212–24220.
- 43 P. E. Hartnett, A. Timalina, H. S. Matte, N. Zhou, X. Guo, W. Zhao, A. Facchetti, R. P. Chang, M. C. Hersam, M. R. Wasielewski and T. J. Marks, *J. Am. Chem. Soc.*, 2014, **136**, 16345–16356.
- 44 D. Zhao, Q. Wu, Z. Cai, T. Zheng, W. Chen and J. Lu, *Chem. Mater.*, 2016, **28**, 1139–1146.
- 45 W. T. Hadmojo, D. Yim, H. Aqoma, D. Y. Ryu, T. J. Shin, H. W. Kim, E. Hwang, W. D. Jang, I. H. Jung and H.-Y. Jang, *Chem. Sci.*, 2017, **8**, 5095–5100.
- 46 C. Zhang, T. Liu, W. Zeng, D. Xie, Z. Luo, Y. Sun and C. Yang, *Materials Chemistry Frontiers*, 2017, **1**, 749–756.
- 47 P. E. Hartnett, H. S. S. R. Matte, N. D. Eastham, N. E. Jackson, Y. Wu, L. X. Chen, M. A. Ratner, R. P. H. Chang, M. C. Hersam, M. R. Wasielewski and T. J. Marks, *Chem. Sci.*, 2016, **7**, 3543–3555.
- 48 X. Liu, T. Liu, C. Duan, J. Wang, S. Pang, W. Xiong, Y. Sun, F. Huang and Y. Cao, *J. Mater. Chem. A*, 2017, **5**, 1713–1723.
- 49 B. Wang, W. Liu, H. Li, J. Mai, S. Liu, X. Lu, H. Li, M. Shi, C.-Z. Li and H. Chen, *J. Mater. Chem. A*, 2017, **5**, 9396–9401.

- 50 A. D. Hendsbee, S. V. Dayneko, J. A. Pells, J. R. Cann and G. C. Welch, *Sustainable Energy & Fuels*, 2017, **1**, 1137–1147.
- 51 Q. Wu, D. Zhao, J. Yang, V. Sharapov, Z. Cai, L. Li, N. Zhang, A. Neshchadin, W. Chen and L. Yu, *Chem. Mater.*, 2017, **29**, 1127–1133.
- 52 D. Sun, D. Meng, Y. Cai, B. Fan, Y. Li, W. Jiang, L. Huo, Y. Sun and Z. Wang, *J. Am. Chem. Soc.*, 2015, **137**, 11156–11162.
- 53 F. Fernández-Lázaro, N. Zink-Lorre and Á. Sastre-Santos, *J. Mater. Chem. A*, 2016, **4**, 9336–9346.
- 54 M. L. Keshtov, D. Y. Godovsky, F. C. Chen, A. R. Khokhlov, S. A. Siddiqui and G. D. Sharma, *Phys. Chem. Chem. Phys.*, 2015, **17**, 7888–7897.
- 55 R. Mishra, J. M. Lim, M. Son, P. Panini, D. Kim and J. Sankar, *Chem.–Eur. J.*, 2014, **20**, 5776–5786.
- 56 P. Rajasingh, R. Cohen, E. Shirman, L. J. W. Shimon and B. Rybtchinski, *J. Org. Chem.*, 2007, **72**, 5973–5979.
- 57 M. J. Frisch, *et al.*, *Gaussian 09, Revision A. 02*, Gaussian, Inc., Wallingford CT, 2009, see ESI† for a complete citation.
- 58 H. Bin, L. Gao, Z. G. Zhang, Y. Yang, Y. Zhnag, C. Zhnag, S. Chen, L. Xue, C. Yang, M. Xiao and Y. Li, *Nat. Commun.*, 2016, **7**, 13651.
- 59 H. Lin, S. Chen, Z. Li, J. Y. Lai, G. Yang, T. McAfee, K. Jiang, Y. Li, Y. Liu, H. Hu, J. Zhao, W. Ma, H. Ade and H. Yan, *Adv. Mater.*, 2015, **27**, 7299–7304.
- 60 M. M. Mandoc, W. Veurman, L. J. A. Koster, B. De Boer and P. W. M. Blom, *Adv. Funct. Mater.*, 2007, **17**, 2167–2173.
- 61 C. M. Proctor, C. Kim, D. Neher and T.-Q. Nguyen, *Adv. Funct. Mater.*, 2013, **23**, 3584–3594.
- 62 A. Guerrero, S. Loser, G. Garciabelmonte, C. J. Bruns, J. Smith, H. Miyauchi, S. I. Stupp, J. Bisquert and T. J. Marks, *Phys. Chem. Chem. Phys.*, 2013, **15**, 16456–16462.
- 63 Q. Zhang, *et al.*, *Nat. Photonics*, 2015, **9**, 35–41.
- 64 Z. He, C. Zhong, X. Huang, W. Y. Wong, H. Wu, L. Chen, S. Su and Y. Cao, *Adv. Mater.*, 2011, **23**, 4636–4643.
- 65 K. Gao, L. Li, T. Lai, L. Xiao, Y. Huang, F. Huang, J. Peng, Y. Cao, F. Liu, T. P. Russell, R. A. J. Janssen and X. Peng, *J. Am. Chem. Soc.*, 2015, **137**, 7282.
- 66 P. Cheng, M. Zhang, T. K. Lau, Y. Wu, B. Jia, J. Wang, C. Yan, M. Qin, X. Lu and X. Zhan, *Adv. Mater.*, 2017, 1605216.
- 67 Y. Li, X. Liu, F.-P. Wu, Y. Zhou, Z.-Q. Jiang, B. Song, Y. Xia, Z.-G. Zhang, F. Gao, O. Ingnas, Y. Li and L.-S. Liao, *J. Mater. Chem. A*, 2016, **4**, 5890–5897.
- 68 K. Kawashima, Y. Tamai, H. Ohkita, I. Osaka and K. Takimiya, *Nat. Commun.*, 2015, **6**, 10085.
- 69 J. Liu, S. Chen, D. Qian, B. Gautam, G. Yang, J. Zhao, J. Bergqvist, F. Zhang, W. Ma, H. Ade, O. Ingnäs, K. Gundogdu, F. Gao and H. Yan, *Nat. Energy*, 2016, **1**, 16089.
- 70 Y. Li, L. Zhong, B. Gautam, H. J. Bin, J. D. Lin, F.-P. Wu, Z. Zhang, Z.-Q. Jiang, Z. G. Zhang, K. Gundogdu, Y. Lib and L. S. Liao, *Energy Environ. Sci.*, 2017, **10**, 1610–1620.
- 71 J. H. Kim, J. H. Paek, J. H. Lee, J. S. Kim, M. Kim, C. Shim and K. Cho, *J. Mater. Chem.*, 2010, **20**, 7398–7405.
- 72 J. S. Kim, Y. Lee, J. H. Lee, J. H. Park, J. K. Kim and K. Cho, *Adv. Mater.*, 2010, **22**, 1355–1360.